Research Article | Vol. 29, No. 5 / 1 March 2021 / Optics Express 6608
Optics EXPRESS

Spectral analysis of organic LED emitters' orientation in thin layers by resonant emission on dielectric stacks

NORBERT DANZ,[1,*] AGOSTINO OCCHICONE,[2] CHRISTOF PFLUMM,[3] PETER MUNZERT,[1] FRANCESCO MICHELOTTI,[2] AND DIRK MICHAELIS[1]

[1] *Fraunhofer Institute for Applied Optics and Precision Engineering IOF, 07743 Jena, Germany*
[2] *Department of Basic and Applied Science for Engineering, Sapienza University of Rome, 00161 Rome, Italy*
[3] *Merck KGaA, Performance Materials, 64293 Darmstadt, Germany*
[*] *norbert.danz@iof.fraunhofer.de*

Abstract: Purposely tailored thin film stacks sustaining surface waves have been utilized to create a unique link between emission angle and wavelength of fluorescent dye molecules. The knowledge of the thin film stack's properties allows us to derive the intrinsically emitted luminescence spectrum as well as to gain information about the orientation of fluorophores from angularly resolved experiments. This corresponds to replacing all the equipment necessary for polarized spectroscopy with a single smart thin film stack, potentially enabling single shot analyses in the future. The experimental results agree well with those from other established techniques, when analyzing the Rubrene derivative in a 2,4,6-tris(biphenyl-3-yl)-1,3,5-triazine (T2T) host used for the fabrication of optimized organic light-emitting diodes. The findings illustrate how resonant layered stacks can be applied to integrated spectroscopic analyses.

1. Introduction

The orientation of emitters in active organic electronic devices such as organic light-emitting diodes (OLED) remains subject of intense investigations, because preferentially aligned emitters improve the photon out-coupling and thus the total device efficiency [1–5]. Nowadays, such a spontaneous alignment in co-evaporated thin films has been observed for most kinds of emitting layers containing fluorophores [3], phosphors [4] or thermally activated delayed fluorescence [5] emitters. In order to analyze the emitter orientation, the second moment of the orientation distribution of the emitting ensemble is accessed experimentally by the electroluminescence (EL) patterns measured with the OLEDs operated electrically [1] or by photoluminescence (PL) with optically excited single thin films [2]. Whilst the EL approach requires special OLED stacks to be prepared, the thin film PL suffers from a rather low emission of emitters oriented perpendicularly to the interfaces when comparing them with that of the parallel aligned ones because of the density of radiative modes at the emitter position in such a geometry.

Recently, 1D photonic crystals (1DPC) sustaining surface electromagnetic (Bloch) waves have been introduced for fluorescence-based sensing [6]. Such periodic dielectric stacks, which are made of alternating high and low refractive index layers, exploit both the surface wave [7] enhanced excitation rate and the angular redistribution of the emission [8]. Furthermore, strong coupling effects in single-sided micro cavities could be observed [9,10]. In such an emission configuration, the excited molecular state preferentially couples to the modes of the resonant stack. Utilizing leaky modes, which radiate into the substrate of the stack, enables to observe an emission pattern constituted by (i) the near field properties of the emitting state superimposed with (ii) the dispersion of the leaky waves. Because each mode features a unique dispersion, it

#417531 https://doi.org/10.1364/OE.417531
Journal © 2021 Received 16 Dec 2020; revised 30 Jan 2021; accepted 4 Feb 2021; published 17 Feb 2021

Optics EXPRESS

couples photons with energy $\hbar\omega$ to a one-to-one corresponding observation angle in the far-field. Therefore, the dispersion of the surface waves yields a dispersed wavelength spectrum, thus giving rise to a polarization dependent and spectrally resolved detection in angularly observing optical systems [6]. Only very recently, the effect of the emitter orientation on the polarized emission coupled to such surface modes began to be addressed more in detail, both theoretically [11] and experimentally [12]. In parallel, approaches for miniaturized spectroscopic systems have been put forth using integrated [13,14] or classical approaches [15–17] in order to achieve portable, hand-held spectroscopy and/or to reach hyperspectral imaging capabilities.

The present work explores the option to utilize the concept of surface wave enhanced luminescence excitation and tailored angular emission distribution for emitter orientation analysis. Such an approach can ultimately simplify complicated PL set-ups by potentially replacing all spectrally dispersing and polarization sensitive elements with an appropriate thin film system. In result, miniaturized polarization resolved spectroscopy [18] might be achieved. Compared to other schemes, such an approach would achieve spectral resolution without requiring lateral patterning [13,14] but exploiting the coupling of the emitter's near field with the leaky waves of the stratified system. In this paper, the PL emission pattern of thin emitting films on top of a purposely designed thin film stack is analyzed, which yields both the intrinsic spectrum and the emitter orientation of the active fluorophores. The results are compared to those obtained with the other established PL approaches well.

2. Experimental system

Figure 1(a) summarizes the approach of angular photoluminescence pattern analysis reported here. The special thin film stack samples purposely deposited for this study on flat glass substrates were mounted in a total internal reflection optical scheme. The back face of the sample was immersion oil coupled to a 45° BK7 prism (n_{BK7}=1.519 at λ_0=550 nm) that was mounted on a rotation stage. Such a configuration allows to extract the light emission coupled to the leaky surface modes of the stack and radiated into the substrate. As sketched in Fig. 1(a), the transition dipole moments of the emitters in the active layer of the stack can be decomposed along the directions perpendicular ($\perp$) and parallel ($\parallel$) to the stack.

Fourier imaging by a cylindrical lens pair provides angularly resolved detection of the spontaneously emitted luminescence pattern at θ_E. The use of an additional linear polarizer allows to observe both emitted polarizations independently. A long pass spectral filter suppresses detection of excitation light.

Concerning photo-excitation, the beam from a collimated laser diode at 404 nm is band pass filtered to remove any residual parasitic luminescence, polarization controlled by a half wave plate and focused by a low divergence cylindrical lens L (f_L=100 mm) onto the stack. The excitation angle θ_I was adjusted by rotating the prism/sample combination. Luminescence excitation and collection are carried out in the (same) plane of incidence. The cylindrical optics allows to excite and collect the emission from a narrow strip aligned perpendicularly with respect to the incidence plane.

Figure 1(b) sketches the idealized case when the dispersion of two surface wave modes of the stack is linear and unique in the (λ,θ) plane. The dispersion of the modes is exploited to extract spectral information from solely angular measurements. In fact, the spectrally broad emission I_{EML} of the emitters can couple to both modes and is radiated into two separate angular ranges, thus enabling to convert angular data into spectral data directly.

When the modes sketched in Fig. 1(b) exhibit a different polarization, the analysis can be extended to molecular orientation information as well. With reference to the sketch shown in Fig. 1(a) and according to basic theoretical considerations [19,20], the $\perp$ component of the absorption/emission dipole moment can couple to the TM polarized surface mode of the stack only. On the other hand, the || component of the dipole moments can couple to both TM and

Optics EXPRESS

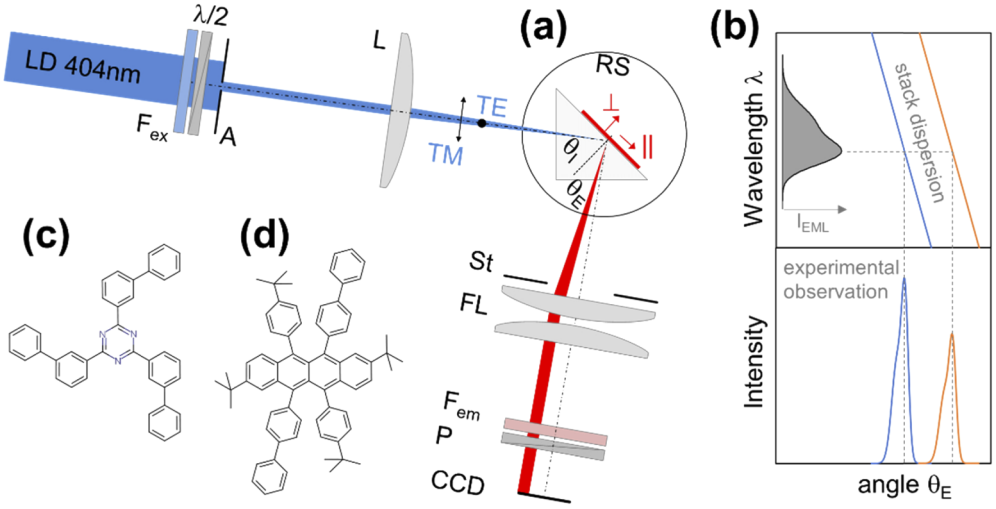

Fig. 1. (a) Experimental system illuminated with laser diode (LD), spectral excitation filter (F_{ex}), half wave plate ($\lambda/2$), aperture (A), cylindrical illumination lens (L), prism mounted on rotation stage (RS), beam stop (St), Fourier observation lens pair (FL), emission filter (F_{em}), polarizer (P). Illumination θ_I and emission θ_E angles are measured inside the BK7 prism; the orientation of the two different polarizations (TE, TM) as well as that of the emitting transition dipole components (||, $\perp$) are sketched for convenience. (b) Idealized sketch of the approach, when the dispersion of two modes (blue, orange straight lines) plotted as propagation angle θ vs. wavelength λ translates the intrinsically emitted spectrum (grey inset) into an angularly observable emission pattern. (c) Structures of the T2 T host and (d) of the rubrene derivative used as emitter, which constitute the EML.

TE-polarized surface modes. Comparing the two angular emission patterns for the TE and TM polarized modes enables to extract the $\perp$ and || contributions and to retrieve the average emitters' orientation. Given enough angular separation of the surface modes, the approach, besides providing spectral resolution, might also achieve polarized analysis without utilizing any dedicated polarization filter.

For the proof-of-concept experiments described here, angular intensity patterns were observed polarization resolved. The detection arm was rotated relative to the prism coupler in order to enable stitching of several angular measurements, in case the angular range of a single shot's Fourier spectrum would not suffice. The option of independently rotating both the sample and the detection arms enables to scan either the excitation (θ_I) or the collection (θ_E) angle while keeping the other fixed. Note that all angular values given below refer to the angle(s) θ inside the BK7 prism, i.e., taking both the refraction between the substrate of the samples to the prism as well as the prism-air refraction into account.

Reference experiments according to a standard approach [2] did not utilize thin film stacks in order to verify the emitter orientation independently. They were performed in a similar 404 nm laser diode excitation configuration but making use of immersion coupling with a fused silica half-ball lens adapted to the reference substrates. Furthermore, a fiber spectrometer (Avantes) was utilized to independently measure intrinsic spectrum as well as the emitter's average orientation.

3. Thin film stack

For the application we target, the thin film stacks described here differ substantially from the 1DPC that are usually optimized [6,21] for biosensing with aqueous samples. In that case, the 1DPC are designed to operate in a restricted wavelength range (~100 nm) for the TE polarization

Optics EXPRESS

only. Here, an increased spectral working range of 400-700 nm is required in order to cover the full emission spectrum of the active layer in an OLED as well as the excitation wavelength.

Thin film metal/dielectric stacks have recently been proposed for achieving angularly dispersed spectra. In particular, metal insulator metal structures have been used for sensing [22] and broadband characterization of the modal spectrum [23]. Here, in order to avoid absorption losses associated with metal microcavities and to enable effective operation in the short visible wavelength range as well, specifically designed periodic fully dielectric 1DPC have been utilized to fulfill the spectral and polarization requirements of the approach in Fig. 1(b). We used Ta_2O_5 and SiO_2 as materials for the high (H) and low (L) index layers, respectively. Searching for a band gap around λ_0=550 nm for both polarizations yields thicknesses of the layers d_H=85 nm and d_L=220 nm corresponding to the stack period $\Lambda=d_H+d_L$=305 nm. The resulting emission angle at λ_0 is about $\theta_E\approx53°$, which is well above the critical angle for total internal reflection as a prerequisite for surface mode propagation and well below any grazing emission condition.

Figure 2 shows the results of the numerical simulations of the photonic band structure and luminescence emission pattern of such a periodic stack for two different cases. Figures 2(a-c) and Fig. 2(d-f) refer to the cases in which the 1DPC is terminated either by a low (Fig. 2(c)) or by a high (Fig. 2(f)) refractive index uppermost layer, respectively.

The photonic band structures were calculated by means of an iterative plane wave eigen–solver method [24] for an infinitely extended 1DPC. The permitted (grey) and forbidden (white) bands are shown for the TE polarization in Fig. 2(a) and for the TM polarization in Fig. 2(d). Since they are calculated for an infinite 1DPC, they apply to both types of termination. A wide gap for TE polarization is found in the spectral region of interest, whereas the corresponding TM band vanishes at the Brewster condition, thus giving rise to a much more restricted spectral range of the available modes.

The dispersions of the TE and TM surface waves can be calculated by means of the transfer matrix method [25] applied to the truncated 1DPC. In the first case, the truncated stack depicted in Fig. 2(c) sustains a Bloch surface wave, which extends across the desired spectral range and exhibits all the desired features. These are the enhanced field at the surface and an almost linear dispersion in the (λ,θ) plane as apparent from Fig. 2(a) (blue line). Unfortunately, there is no TM polarized counterpart apparent in such a structure. However, a surface wave with TM polarization is found for the second stack sketched in Figs. 2(f), whose dispersion is shown in Fig. 2(d) (blue line). Like the first case, using this kind of periodic stack with a high index top layer does not exhibit a TE polarized surface wave.

In the Figs. 2(b,e) we show the numerical calculations of the emission patterns for the two cases. The simulations were carried out by applying a transfer matrix formulation [25,26] of the Green's function approach [19] for an emitting dipole oriented isotropically at the surface of the 1DPC and characterized by a constant emission spectrum. A unitary intrinsic quantum efficiency as well as a constant photon generation rate for all positions inside the active layer is assumed. The results illustrate that simultaneous coupling of the emission to both a TE and a TM polarized surface mode cannot be obtained in any of the two cases. On other hand, the two different terminations can give rise to coupling of the spontaneous emission only and exclusively to either the TE or the TM modes.

The precedent observations suggest that it is necessary to relax the constraint on the periodicity of the stack in order to achieve a satisfactory dispersive characteristic of the thin film system. In result, a high index "waveguiding" layer is combined with a low index (SiO_2) separation layer and a periodic stack to control the leakage of the field into the substrate. This waveguiding layer consists of the organic thin film under test (~30 nm thickness) and a high index dielectric layer (~55 nm thickness). Furthermore, the thin film stack was tailored carefully to adjust the quality factors Q of the surface waves, without however reaching the condition in which they may cause reabsorption issues, modifications of the out-coupled spectrum, or limitations due to

Optics EXPRESS

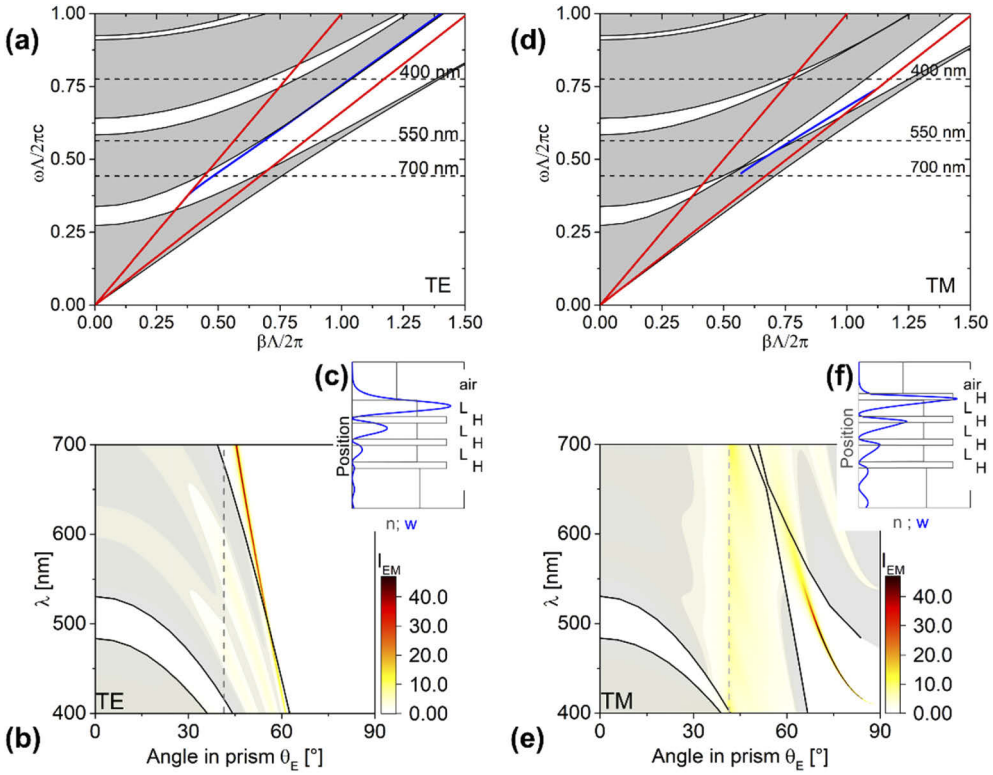

Fig. 2. Simulations for periodic thin films stacks in TE (a, b, c) and TM (d, e, f) polarization, calculated for constant refractive index values at λ_0=550 nm. Diagrams (a, d) show the photonic band structures along with the air (upper) and substrate (lower) light lines (red) and the surface mode dispersion (blue). The permitted and forbidden bands are colored in grey and white, respectively; β denotes the in-plane propagation constant. Surface mode dispersions have been obtained for the structures depicted in diagrams (c, f), which also plot for convenience the modes' energy density distributions w calculated when the 1DPC is excited at λ_0 = 550 nm and at resonant angle from the substrate side. Diagrams (b, e) show the corresponding spontaneous emission patterns in the substrate plotted in the λ-θ-plane, whose false color representation is superimposed to the band structures. The black lines illustrate the photonic band's edges and the dashed line indicates the air light line for convenience.

Optics EXPRESS

the collection field of view [27]. Therefore, the dielectric part of the high index "waveguiding" layer is made of TiO_2 in order to introduce small absorption losses which limit the propagation length of the surface modes. Taking the optical properties of the medium under consideration into account additionally yields the stack listed in Table 1. The mode distributions and the dispersion properties are summarized in Fig. 3, which shows the calculated emission patterns for either ∥ or ⊥ aligned emitters in the EML. In the angular range experimentally explored in the present work $\theta_E \in (42°,72°)$, the patterns are dominated by two main surface modes with different polarization (TE and TM) that feature a strong excitation by the emitters in the EML. As the intensity distributions in Figs. 3(a,d) indicate, the energy density maxima of the major TM mode are located in the high index layers, whilst those for TE lay in the low index materials. A lower order TE mode with higher propagation constant is also observed at large angles and wavelengths (λ~690 nm and θ~82°), which exhibits intensity maxima in the high index layers. Because the brightness of the main TE and TM modes is connected to their higher/lower localization in the EML, this stack design yields comparable emission intensity levels for both polarizations rather than a single dominant polarization. The simulations confirm that the ⊥ component can couple only to the main TM surface wave, while the ∥ component couple to both the main TE and TM modes. They also show that the specific design of the stack given in Table 1 allows to angularly resolve the emission coupled to the main TE and TM modes, since their dispersions are well separated along the θ_E direction. In Fig. 3, we also mark the angles that were used to excite luminescence at 404 nm in the experiments. The labels TE1/2 and TM1/2 are just used to identify such positions and do not refer to a mode order classification.

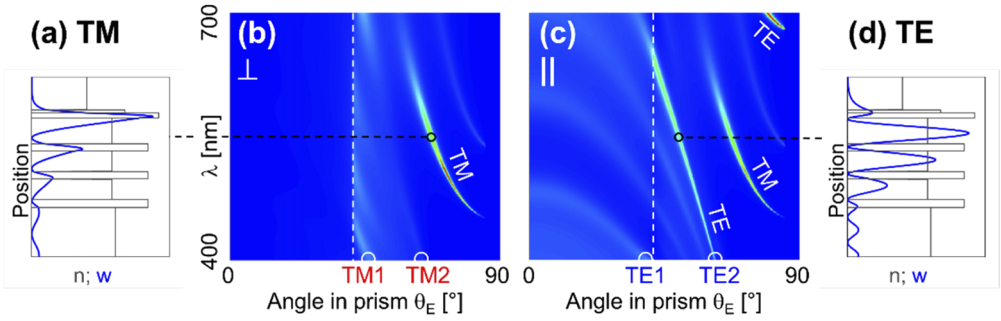

Fig. 3. Illustration of the final stack's (compare Table 1) properties. Simulated profiles of the energy density w at λ=550 nm for the modes utilized in TM at θ_E=67.2° (a) and in TE polarization at θ_E=49.2° (d); the energy density distribution is superimposed to the refractive index profile of the stack. False color plots illustrate the emission spectra for emitters aligned perpendicularly (b) and parallel (c) to the interfaces of the thin film stack when assuming a constant emitted spectrum. The dashed line indicates the critical angle of total internal reflection at about 42°; due to the reduced refractive index of the AF32 substrate, leaky wave resonances do not reach 90° emission angle inside the prism. The polarization of the major surface modes is indicated in the diagrams as well as the angular positions (TE1/2, TM1/2) of luminescence excitation (compare Fig. 4).

The emitters are embedded in the uppermost layer of the stack with an air cladding. The stack contains a periodic part made of low loss Ta_2O_5 and SiO_2 layers as well as a high index waveguide part containing the emissive layer (EML). The "lossy" TiO_2 layer adjusts Q and the associated propagation length [27]. All inorganic layers were deposited by plasma ion assisted vacuum evaporation (PIAD) with a Bühler/Leybold Optics APS 904 machine [28]. Stacks were characterized in detail by variable angle spectroscopic ellipsometry (VASE, Sentech) and exhibit the refractive indices given for one example wavelength in Table 1 for convenience. The organic EML was deposited by thermal co-evaporation of 2,4,6-tris(biphenyl-3-yl)-1,3, 5-triazine (T2T

Optics EXPRESS

Table 1. List of the complete thin film stack with designed and measured layer thicknesses d as well as complex refractive indices used for simulation. The EML layer is birefringent uniaxially with ordinary (o) and extraordinary (e) complex refractive indices.

Material	Thickness d [nm]		Refractive index @ λ=550 nm	
	Design	Measured	real part n	imaginary part κ
Air	Cladding		1	
EML	30	33.9	1.688 (o)	4.9×10^{-3} (o)
			1.815 (e)	3.6×10^{-3} (e)
TiO_2	55	55.5	2.313	1.9×10^{-3}
SiO_2	285	287.2	1.453	1×10^{-6}
Ta_2O_5	85	81.7	2.115	5×10^{-5}
SiO_2	220	225.2	1.453	1×10^{-6}
Ta_2O_5	85	83.7	2.115	5×10^{-5}
SiO_2	220	228.9	1.453	1×10^{-6}
Ta_2O_5	85	88.7	2.115	5×10^{-5}
AF32	Substrate		1.513	

[29], Fig. 1(a)) as host doped with 5% of a rubrene derivative [30] (Fig. 1(c)) as emitter. These constituents can be applied in thermally activated delayed fluorescence-based devices [31,32]. The EML layer is birefringent as stated in Table 1. Additionally, reference samples of such an organic EML were evaporated onto fused silica substrates for reference experiments utilizing photoluminescence (PL) of single supported films according to [2].

4. Results

4.1. Angular excitation and emission spectra

Figures 4(a, b) illustrate the angular excitation spectra measured when rotating the sample-prism combination and integrating the TE-polarized emission intensity over the angular range $42°<\theta_E<54°$, which is defined by the aperture of the beam stop (St) and the width of the CCD. Such an experiment reveals optimum angular positions for luminescence excitation and enables to compare the angular spectra with predicted ones in order to validate the parameters (thicknesses and refractive indices) of the thin film stack. Such comparison was achieved by modelling the emission of an (isotropic) emitter ensemble in the EML at the excitation wavelength of 404 nm for convenience. This approach does not allow fitting the absorption spectra directly but suffices to compare the peak positions of the excitation approximately. Obviously, the TE and TM modes marked in Fig. 3 at the excitation wavelength are observed as excitation maxima.

Angular emission spectra have been measured with the excitation at any of the four angle/polarization combinations marked in Figs. 3(b, c) and 4(a, b) while observing both TE- and TM polarized emission for each case (Fig. 4(c, d)). It is worth noting that the shape of the angular emission spectra is almost independent of the excitation, because only the emitted spectra's amplitude varies when altering the excitation conditions.

4.2. Data analysis

The procedure described above has been applied in order to achieve a spectroscopic analysis of the angular data. First, the pronounced TM-polarized emission peak observed in the $58°<\theta_E<72°$ range is associated with a spectral distribution due to the knowledge of the TM-polarized surface wave's dispersion (compare Fig. 3(a)). Therefore, we follow previous approaches [1,4,33] and

Optics EXPRESS

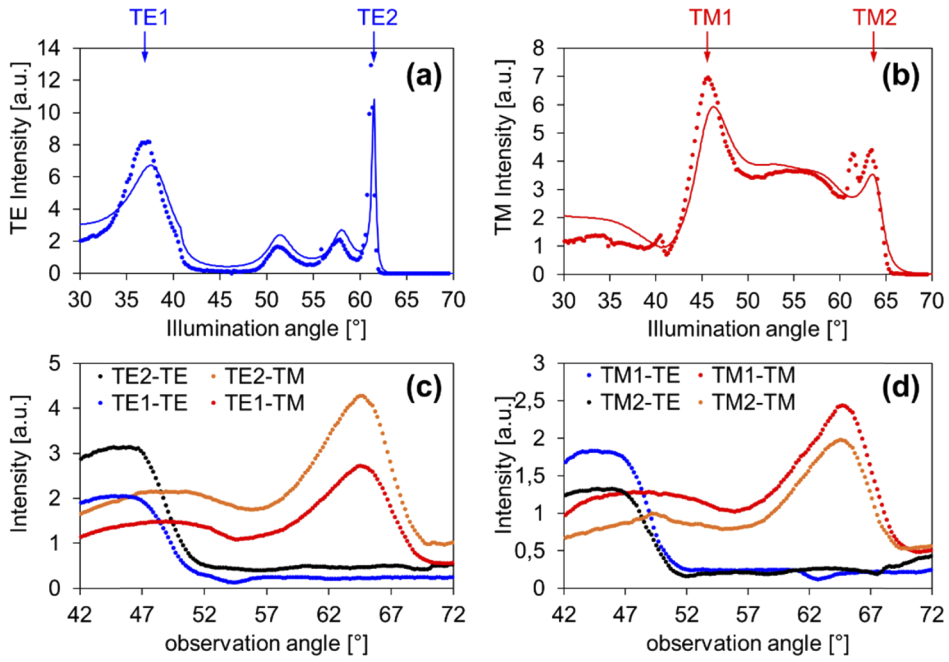

Fig. 4. Angular patterns (a, b) obtained when scanning the excitation angle in case of TE (a) and TM-polarized (b) illumination while integrating TE polarized emission in the $42°<\theta_E<54°$ angular range. Dots are experimental data; the lines depict the simulated distributions (see text for details). Angular emission patterns (c, d) with fixed illumination when exciting in TE (c) or TM (d) polarizations at the angular positions indicated in diagrams (a) and (b).

model the TM-polarized emission pattern by

$$I_{TM}(\theta) \sim \langle p_\perp \rangle^2 \cdot \sum_i \hat{M}_{\perp,TM}(\theta, \lambda_i) \cdot \vec{I}_{int}(\lambda_i) + \langle p_{||} \rangle^2 \cdot \sum_i \hat{M}_{||,TM}(\theta, \lambda_i) \cdot \vec{I}_{int}(\lambda_i) \qquad (1)$$

assuming the intrinsically emitted spectrum $\vec{I}_{int}(\lambda_i)$ and the contribution of perpendicular and parallel emitters according to $\langle p_\perp \rangle^2 \sim \int g(\vartheta) \cdot \cos^2\vartheta \cdot \sin\vartheta \cdot d\vartheta$ and $\langle p_{||} \rangle^2 \sim \int g(\vartheta) \cdot \sin^2\vartheta \cdot \sin\vartheta \cdot d\vartheta$, respectively, with the orientation distribution of the emitting ensemble $g(\vartheta)$ [1,4]. The polarized emission patterns $\hat{M}(\theta, \lambda_i)$ were obtained when assuming a constant profile of the emission zone and have been generated by means of the established Green's function method [19] using self-written tools (compare Refs. [25,26,33] for details).

Both the emitter orientation $\langle p_{||} \rangle^2 : \langle p_\perp \rangle^2$ as well as the intrinsically emitted spectrum $\vec{I}_{int}(\lambda_i)$ are unknow and need to be extracted from the angular spectra. Considering that the emission pattern is governed by the dispersion of the stack, i.e. the system's geometry, Eq. (1) can be inverted based on an approximation for the emitter orientation in order to extract $\vec{I}_{int}(\lambda_i)$. Because direct deconvolution fails due to the ill-posed problem, we use a part of the emission pattern in Fig. 3(a) to compute the pseudo-inverse matrix of $\langle p_\perp \rangle^2 \hat{M}_{\perp,TM}(\theta, \lambda_i) + \langle p_{||} \rangle^2 \hat{M}_{||,TM}(\theta, \lambda_i)$ on a 500 nm$\leq \lambda \leq$700 nm with $\Delta\lambda$=5 nm and $57° \leq \theta_E \leq 72°$ with $\Delta\theta_E$=0.2° mesh by restricting to the ten highest eigenvalues. Higher order terms, i.e., eigenfunctions with more than ten zeros in the spectral range considered, introduce quickly oscillating terms into the deconvolution result and thus are dropped. This approach is reasonable because no quickly oscillating behavior is expected for the present dye. Its photoluminescence (PL) spectrum is shown in Fig. 5(a) as obtained from measurements with single supported films by the method according to Ref. [2].

Optics EXPRESS

Applying this procedure to all four TM-polarized angular data sets of Fig. 4(c, d) yields the spectral data illustrated in Fig. 5(a).

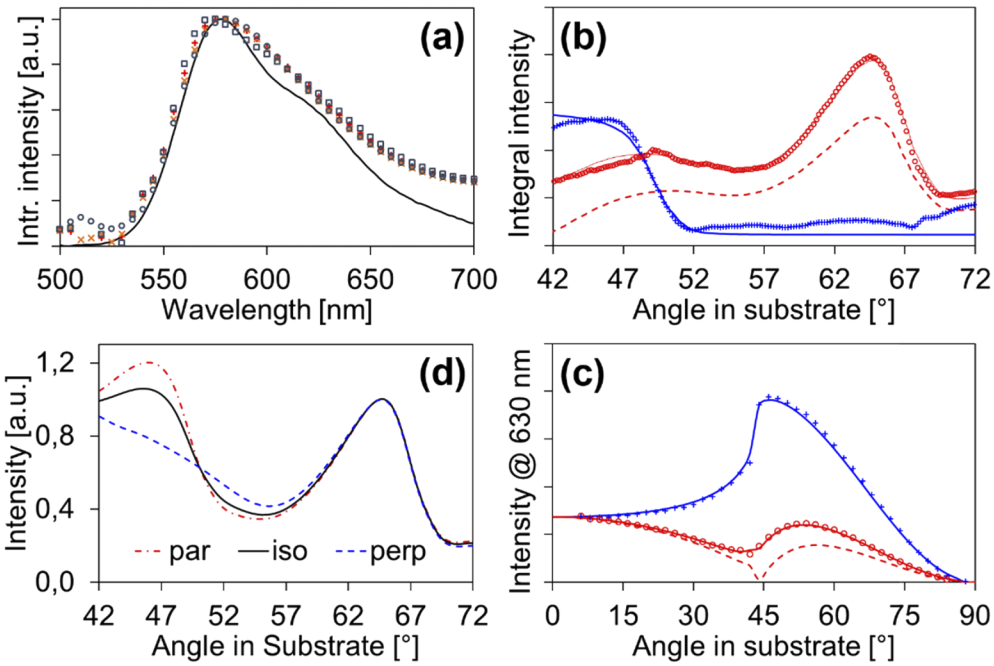

Fig. 5. (a) Deconvoluted spectra obtained from the TM polarized emission for four different excitation conditions (symbols) as well as a PL spectrum (black line) of the same material for comparison. (b, c) Fitted angular intensity distribution for orientation analysis obtained for spectrally integrated, BSW coupled emission (b) and monochrome PL emission of 30 nm thin film on a glass substrate (c). Both diagrams show TE (blue crosses) and TM (red circles) experimental data along with the corresponding fits (straight lines). The dashed red curve illustrates the TM pattern for strictly parallel emitters. (d) Simulated unpolarized emission of the present dye when assuming a parallel (dash dot), an isotropic (straight) and a perpendicular (dash) orientation of emitting dipoles. The curves are normalized onto the TM polarized peak for better comparability.

Obviously, the short wavelength edge as well as the wavelength of maximum emission agree well with the PL spectrum obtained from a single film. Data in the long wavelength range λ>600 nm yield an increasing difference to the reference spectrum with increasing wavelength. This is attributed to the decreasing emission intensity in this wavelength range, which limits the deconvolution accuracy. However, all four experiments yield similar intrinsic spectra that deviate by less than 5% only in the wavelength range 550 nm<λ<700 nm. Therefore, the averaged result of these spectra was assumed for fitting the angular patterns.

Next, the angular spectra need to be fitted for both polarizations in order to extract emitter orientation. Similar to Eq. (1) the TE-polarized emission pattern is modelled according to

$$I_{TE}(\theta) \sim \langle p_{||} \rangle^2 \cdot \sum_i \hat{M}_{||,TE}(\theta, \lambda_i) \cdot \vec{I}_{int}(\lambda_i) \tag{2}$$

because TE polarized emission originates from the parallel components of the dipole transition moments solely. Due to the angularly separated emission of TE and TM polarization, the fitted range has been restricted to 42°<θ_E<53° and 55°<θ_E<72° to cover the TE- and TM polarized surface wave coupled emission, respectively. Figure 5(b) illustrates the result for the data obtained

Optics EXPRESS

with TM2 excitation. We find an orientation ratio $\langle p_{||}\rangle^2$:$\langle p_{\perp}\rangle^2$=2:(0.85 ± 0.08) as the average orientation obtained in the four experiments with different excitation conditions. The reference experiments based on angularly and spectrally resolved PL analysis on single thin films on fused silica samples yields emission patterns like the example plotted in Fig. 5(c) corresponding to an emitter orientation of $\langle p_{||}\rangle^2$:$\langle p_{\perp}\rangle^2$=2:(0.82 ± 0.03). We attribute the increased error in our approach to deviations between the real stack geometry and the one assumed for data analysis.

5. Conclusion

In conclusion, a thin film stack has been designed, prepared and characterized to be used in an integrated spectroscopic application. The thin film system sustains leaky waves featuring a large amplitude near the stack's surface. Active molecules at the stack's surface preferably emit into the surface modes, thus giving rise to pronounced, angularly separated TE- and TM-polarized emission patterns. Due to the known dispersion of the surface waves, angular emission can be deconvoluted to extract the dye's intrinsically emitted spectrum. Utilizing this knowledge allows to fit both TE- and TM-polarized emission and to extract orientation information about the emitter's orientation distribution. The results derived for an OLED singlet emitting film correspond with those obtained in a standard experiment well.

Such an approach illustrates one example to exploit the properties of surface wave coupled emission for spectroscopic applications. Depending on the spectral range and polarization properties considered, all bulky wavelength and polarization sensitive elements of standard approaches can be replaced by a smart substrate coated with a properly designed resonant thin film system. This stack features both an angularly separated and polarized emission as well as a preferred emission into the localized modes of the system, thus narrowing the angular range of emission from 0°. . . 90° (standard PL) down to 45°. . . 70°. When observing the emission without polarizer, such as illustrated in Fig. 5(d), the broad peak in the 60°..70° range allows to extract the spectrum whilst the pattern shape in the 42°..58° angular range visualizes orientation properties. But the contrast for different emitter orientations decreases when comparing it to the polarized observation case. This is attributed to the fact that a TM emission background is present in the angular range of TE emission, the intensity of which has been utilized to extract emitter orientation.

Future work might improve the polarization contrast of the stack and further improve this type of angularly and spectrally dispersed emitting systems. This could result in active devices with a frequency dependent angular spectrum for potential applications [18] in integrated spectroscopic devices. Furthermore, the one-dimension angular resolution we achieved here to extract the orientation ratio via the polarization can be extended to a two-dimensional Fourier plane microscopy observation, opening the way towards the characterization of two-dimension semiconductor systems [34] and, in the case of OLED devices [35], extend the analysis onto potential in-plane anisotropies.

Funding. Sapienza Università di Roma; Ministero dell'Istruzione, dell'Università e della Ricerca (ARS01_00769); Regione Lazio (85-2017-14945); Horizon 2020 Framework Programme (732013).

Disclosures. CP: Merck KGaA Darmstadt, Germany (E), ND: Fraunhofer IOF Jena, Germany (P, R)

References

1. M. Flämmich, M. C. Gather, N. Danz, D. Michaelis, A. H. Bräuer, K. Meerholz, and A. Tünnermann, "Orientation of emissive dipoles in OLEDs: Quantitative in situ analysis," Org. Electron. **11**(6), 1039–1046 (2010).
2. J. Frischeisen, D. Yokoyama, C. Adachi, and W. Brütting, "Determination of molecular dipole orientation in doped fluorescent organic thin films by photoluminescence measurements," Appl. Phys. Lett. **96**(7), 073302 (2010).
3. D. Yokoyama, A. Sakaguchi, M. Suzuki, and C. Adachi, "Horizontal orientation of linear-shaped organic molecules having bulky substituents in neat and doped vacuum-deposited amorphous films," Org. Electron. **10**(1), 127–137 (2009).
4. M. Flämmich, J. Frischeisen, D. S. Setz, D. Michaelis, B. C. Krummacher, T. D. Schmidt, W. Brütting, and N. Danz, "Oriented phosphorescent emitters boost OLED efficiency," Org. Electron. **12**(10), 1663–1668 (2011).

Optics EXPRESS

5. C. Mayr, S. Y. Lee, T. D. Schmidt, T. Yasuda, C. Adachi, and W. Brütting, "Efficiency Enhancement of Organic Light-Emitting Diodes Incorporating a Highly Oriented Thermally Activated Delayed Fluorescence Emitter," Adv. Funct. Mater. **24**(33), 5232–5239 (2014).
6. A. Sinibaldi, A. Fieramosca, R. Rizzo, A. Anopchenko, N. Danz, P. Munzert, C. Magistris, C. Barolo, and F. Michelotti, "Combining label-free and fluorescence operation of Bloch surface wave optical sensors," Opt. Lett. **39**(10), 2947–2950 (2014).
7. P. Yeh, A. Yariv, and C.-S. Hong, "Electromagnetic propagation in periodic stratified media. I. General theory," J. Opt. Soc. Am. **67**(4), 423–438 (1977).
8. M. Ballarini, F. Frascella, F. Michelotti, G. Digregorio, P. Rivolo, V. Paeder, V. Musi, F. Giorgis, and E. Descrovi, "Bloch surface waves-controlled emission of organic dyes grafted on a one-dimensional photonic crystal," Appl. Phys. Lett. **99**(4), 043302 (2011).
9. S. Pirotta, M. Patrini, M. Liscidini, M. Galli, G. Dacarro, G. Canazza, G. Guizzetti, D. Comoretto, and D. Bajoni, "Strong coupling between excitons in organic semiconductors and Bloch surface waves," Appl. Phys. Lett. **104**(5), 051111 (2014).
10. S. Hou, Y. Qu, X. Liu, and S. R. Forrest, "Ultrastrong coupling of vibrationally dressed organic Frenkel excitons with Bloch surface waves in a one-sided all-dielectric structure," Phys. Rev. B **100**(4), 045410 (2019).
11. F. Michelotti and E. Sepe, "Anisotropic Fluorescence Emission and Photobleaching at the Surface of One Dimensional Photonic Crystals Sustaining Bloch Surface Waves. I. Theory," J. Phys. Chem. C **123**(34), 21167–21175 (2019).
12. E. Sepe, A. Sinibaldi, N. Danz, P. Munzert, and F. Michelotti, "Anisotropic Fluorescence Emission and Photobleaching of Fluorophores in Proximity of One Dimensional Photonic Crystals Sustaining Bloch Surface Waves. II. Experiments," J. Phys. Chem. C **123**(34), 21176–21184 (2019).
13. B. Redding, S. F. Liew, R. Sarma, and H. Cao, "Compact spectrometer based on a disordered photonic chip," Nat. Photonics **7**(9), 746–751 (2013).
14. J. Bao and M. G. Bawendi, "A colloidal quantum dot spectrometer," Nature **523**(7558), 67–70 (2015).
15. T. C. Wilkes, A. J. S. McGonigle, J. R. Willmott, T. D. Pering, and J. M. Cook, "Low-cost 3D printed 1 nm resolution smartphone sensor-based spectrometer: instrument design and application in ultraviolet spectroscopy," Opt. Lett. **42**(21), 4323–4326 (2017).
16. A. J. Das, A. Wahi, I. Kothari, and R. Raskar, "Ultra-portable, wireless smartphone spectrometer for rapid, nondestructive testing of fruit ripeness," Sci. Rep. **6**(1), 32504 (2016).
17. N. Danz, B. Höfer, E. Förster, T. Flügel-Paul, T. Harzendorf, P. Dannberg, R. Leitel, S. Kleinle, and R. Brunner, "Miniature integrated micro-spectrometer array for snap shot multispectral sensing," Opt. Express **27**(4), 5719–5728 (2019).
18. N. Danz and C. Wächter, Patent Application WO2016/012276.
19. R. R. Chance, A. Prock, and R. Silbey, "Molecular fluorescence and energy transfer near interfaces," Adv. Chem. Phys. **37**, 1–65 (1978).
20. K. A. Neyts, "Simulation of light emission from thin-film microcavities," J. Opt. Soc. Am. A **15**(4), 962–971 (1998).
21. P. Lova, G. Manfredi, and D. Comoretto, "Advances in Functional Solution Processed Planar 1D Photonic Crystals," Adv. Opt. Mater. **6**(24), 1800730 (2018).
22. T.-H. Lan, Y.-K. Chung, J.-E. Li, and C.-H. Tien, "Plasmonic rainbow rings induced by white radial polarization," Opt. Lett. **37**(7), 1205–1207 (2012).
23. S. Cao, M. Achlan, J.-F. Bryche, P. Gogol, G. Dujardin, G. Raseev, and E. Le Moal, "An electrically induced probe of the modes of a plasmonic multiplayer stack," Opt. Express **27**(23), 330011 (2019).
24. S. G. Johnson and J. D. Joannopoulos, "Block-iterative frequency-domain methods for Maxwell's equations in a plane wave basis," Opt. Express **8**(3), 173–190 (2001).
25. N. Danz, R. Waldhäusl, A. Bräuer, and R. Kowarschik, "Dipole lifetime in stratified media," J. Opt. Soc. Am. B **19**(3), 412–419 (2002).
26. D. S. Setz, T. D. Schmidt, M. Flämmich, S. Nowy, J. Frischeisen, B. C. Krummacher, T. Dobbertin, K. Heuser, D. Michaelis, N. Danz, W. Brütting, and A. Winnacker, "Comprehensive efficiency analysis of organic light-emitting devices," J. Photonics Energy **1**(1), 011006 (2011).
27. F. Michelotti, R. Rizzo, A. Sinibaldi, P. Munzert, C. Wächter, and N. Danz, "Design rules for combined label-free and fluorescence Bloch surface wave biosensors," Opt. Lett. **42**(14), 2798–2801 (2017).
28. P. Munzert, N. Danz, A. Sinibaldi, and F. Michelotti, "Multilayer coatings for Bloch surface wave optical biosensors," Surf. Coat. Technol. **314**, 79–84 (2017).
29. H.-F. Chen, S.-J. Yang, Z.-H. Tsai, W.-Y. Hung, T.-C. Wang, and K.-T. Wong, "1,3,5-Triazine derivatives as new electron transport–type host materials for highly efficient green phosphorescent OLEDs," J. Mater. Chem. **19**(43), 8112–8118 (2009).
30. W. C. H. Choy, Y. S. Wu, C. H. Chen, and K. W. Cheah, "Optical properties of a novel yellow fluorescent dopant for use in organic LEDs," Appl. Phys. A **81**(3), 517–521 (2005).
31. H. Nakanotani, K. Masui, J. Nishide, T. Shibata, and C. Adachi, "Promising operational stability of high-efficiency organic light-emitting diodes based on thermally activated delayed fluorescence," Sci. Rep. **3**(1), 2127 (2013).
32. H. Nakanotani, T. Higuchi, T. Furukawa, K. Masui, K. Morimoto, M. Numata, H. Tanaka, Y. Sagara, T. Yasuda, and C. Adachi, "High-efficiency organic light-emitting diodes with fluorescent emitters," Nat. Commun. **5**(1), 4016 (2014).

Optics EXPRESS

33. N. Danz, M. Flämmich, D. S. Setz, B. C. Krummacher, D. Michaelis, and T. Dobbertin, "Detection of sub-10 nm features in organic light-emitting diodes," Opt. Lett. **37**(19), 4134–4136 (2012).
34. D. Pommier, R. Bretel, L. E. P. Lopez, F. Fabre, A. Mayne, E. Boer-Duchemin, G. Dujardin, G. Schull, S. Berciaud, and E. Le Moal, "Scanning tunneling microscope-induced excitonic luminescence of a two-dimensional semiconductor," Phys. Rev. Lett. **123**(2), 027402 (2019).
35. J. Kim, H. Zhao, S. Hou, M. Khatoniar, V. Menon, and S. R. Forrest, "Using Fourier-plane imaging microscopy for determining transition-dipole-moment orientations in organic light-emitting diodes," Phys. Rev. Appl. **14**(3), 034048 (2020).